Journal of Crystal Growth 453 (2016) 20–26

Contents lists available at ScienceDirect

Journal of Crystal Growth

journal homepage: www.elsevier.com/locate/jcrysgro

Effect of the capillary meniscus height on the instability of large Prandtl number Czochralski melt flow

E. Miroshnichenko, E. Kit, A. Yu. Gelfgat *

School of Mechanical Engineering, Faculty of Engineering, Tel-Aviv University, Ramat Aviv, Tel-Aviv 69978, Israel

ARTICLE INFO

Article history:
Received 1 June 2016
Received in revised form
26 July 2016
Accepted 28 July 2016
Communicated by: Pierre Müller
Available online 2 August 2016

Keywords:
A1. Fluid flows
Convection
Heat transfer
A2. Czochralski method

ABSTRACT

Effect of the capillary meniscus on the instability of large Prandtl number Czochralski melt flow is studied experimentally. The measurements are conducted in two experimental facilities by two independent non-intrusive optical techniques. The quantitative results are presented as dependencies of the critical Grashof number (critical temperature difference) on the meniscus height for different Prandtl numbers, radii and aspect ratios. The results show that with increase of the meniscus height the critical temperature difference noticeably grows and sometimes doubles. Recently reported parametric relations for the critical Grashof number and oscillations frequency are extended to include parameters of the meniscus.

1. Introduction

Effect of the capillary meniscus on the Czochralski and similar crystal growth processes is well-known. The most recent review of the relevant issues is given in book [1]. Additionally, recent study [2] discusses effect of the meniscus on spiral growth of oxide crystals, whose Prandtl number is large and sometimes exceeds the value of 10. One of important factors that can be affected by the meniscus shape is pattern of the Czochralski melt flow and, especially, it stability. The latter is the main object of the present experimental study.

Laboratory modeling of instabilities in Czochralski melt flow is performed for more than 30 years starting from experiments of Jones [3], however most of them do not mention parameters of the meniscus or its effect. In 2001, Hintz et al. [4,5] stated that meniscus effects on Czochralski melt flow have not been studied experimentally and showed that after onset of flow instability the oscillation frequency depends on the meniscus height. To the best of our knowledge this issue was not addressed since then. To avoid discussion of these effects, in our recent experiments [6] the meniscus height was always fixed at 1.25 mm.

In the current study we extend previous model experiments [4–8] to an examination of the meniscus height effect on the instability in large Prandtl number Czochralski melt flow. The experiments are performed on two experimental setups designed to keep all the characteristic lengths at a ratio 1:1.9. We show that with the increase of the meniscus height the critical temperature difference (the critical Grashof number) tends to grow. Depending on other system parameters the growth is sometimes slow, but in other cases the critical temperature differences double. At large heights, just before the meniscus breaks, the critical temperature difference decrease, which can be attributed to an abrupt change of the meniscus shape. We observe that the frequency of flow oscillations, which develop after the instability onset, also grows with the increase of the meniscus height.

Further examination of results shows that in spite all the characteristic lengths in the two setups scaled geometrically as 1:1.9, the critical temperature difference does not scale as $1:1.9^3$, as could follow from the definition of the Grashof number. Also, the dimensionless oscillations frequencies do not scale as $1:1.9^2$ as one could expect basing on the viscous or thermal diffusive time scales. Absence of the expected scaling shows that the results are possibly affected by the parameters related to the capillary phenomena: the Marangoni and Bond numbers, the dimensionless meniscus height, and the wetting angle. Effects of these parameters, as well as other possible reasons, are discussed. Finally, we extend the scaling relations of [6] to include the Bond number and the dimensionless meniscus height.

2. Experimental setups

Measurements were carried out on two experimental setups, in

* Corresponding author.
E-mail address: gelfgat@tau.ac.il (A.Yu. Gelfgat).

http://dx.doi.org/10.1016/j.jcrysgro.2016.07.041
0022-0248/

which two sapphire crucibles with the radii of 20 and 38 mm were installed. In both setups the crucibles are heated by running hot water. The smaller experimental setup has copper crystal dummies of different radii attached to a copper rod, which is cooled by running cold water, and resembles one used in our recent study [6]. In the larger setup, cold water runs inside the dummy as it was implemented in [8]. The water temperatures are controlled by the isothermal bathes that provide the temperature resolution of 0.1 °C, and additionally by the thermocouples placed inside the hot and cold water chambers. The experimental liquids are four silicone oils whose viscosity is 2, 5, 10, and 20 cSt. Their Prandtl numbers are 23.9, 57.9, 99.3, and 206, respectively, and the other physical properties are listed in [9]. In both setups the meniscus height was controlled by a specially constructed microcontroller-based device with the analog-to-digital converter integrated in the microcontroller, and the digital display. The vertical movement of the cupper rods with the attached crystal dummies was monitored by a linear potentiometer whose resistance is converted to millimeters. The meniscus height was varied between 0 and 1.75 mm in the smaller setup and between 0 and 2.25 mm in the larger one. This variation allowed us to obtain four qualitatively different meniscus positions of the crystal dummy, as is sketched in Fig. 1. The meniscus can be attached to the crystal side (curve 1), which apparently happens at zero meniscus height and in the top-seeded solution growth (TSSG) [10]. It can be attached to the crystal dummy edge (curves 2 and 3), where the curve 2 describes the meniscus shape for a stable Czochralski process. When the height is larger the meniscus is attached to the bottom surface of the dummy (curve 4). This may happen in the case of the spiraling growth, as is described in [2].

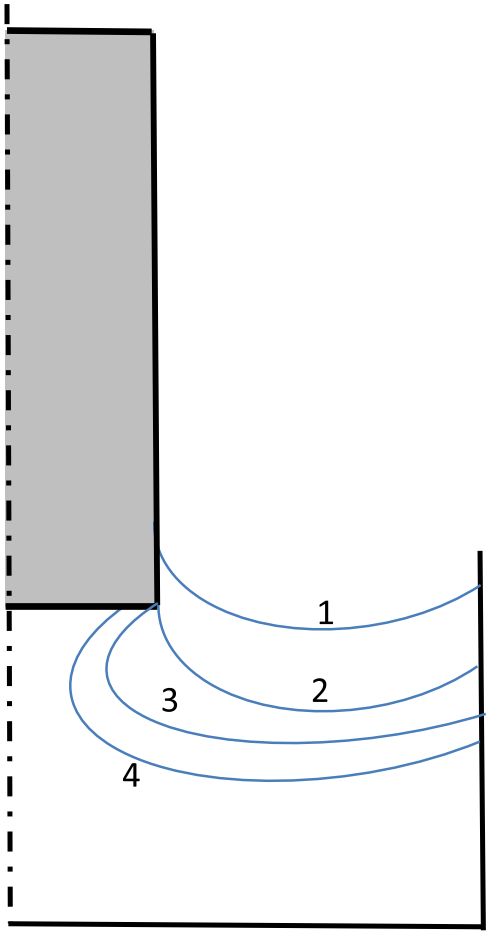

Fig. 1. Sketch of possible meniscus shapes: 1 – attached to the side of the crystal dummy, 2 – attached to the edge of the crystal dummy described by a single-valued function $z(r)$, 3 – attached to the edge of the crystal dummy described by a double-valued function $z(r)$, and 4 – attached to the bottom of the crystal dummy.

As in our previous study [6], the measurements of instability onset were completely non-intrusive and made by two independent and self-cross-verifying optical techniques. The techniques are based on digital post-processing of the time-dependent Schlieren images and monitoring of the time-dependent laser beam deflection, as described in [6], to where the reader is referred for further details.

3. Menisci shape numerical modeling

To get a qualitative impression of how the menisci shape changes, we carried out several numerical calculations. Calculation of the meniscus for all three cases of Fig. 1 is rather difficult problem, as described and discussed in [1]. However, for the case of curve 2 the meniscus can be computed relatively easy. Assuming that $R_{crystal}$, $R_{crucible}$, H, and h_m are the crystal and the crucible radii, the height of the melt without crystal, and the height of the meniscus above H, respectively, we look for a meniscus shape function $z(r)$ that satisfies the Laplace-Young equation (all the lengths are scaled by the crucible radius $R_{crucible}$)

$$\frac{z_{rr}''}{\left(1+z_r'^2\right)^{3/2}}+\frac{z_r'^2}{r\left(1+z_r'^2\right)^{1/2}}+Bo(z-z_0)=0 \tag{1}$$

with the restriction on volume conservation

$$\pi(A+h)R_{crystal}^2+2\pi\int_R^1 rz(r)dr=\pi A \tag{2}$$

and the boundary conditions

$$z(R)=A+h, \tag{3}$$

$$z_r'(1)=\tan(\alpha) \tag{4}$$

Here $A=H/R_{crucible}$ is the melt aspect ratio, $R=R_{crystal}/R_{crucible}$ is the crystal/crucible radii ratio, $h=h_m/R_{crucible}$ is the relative meniscus height, α is the wetting angle at the crucible wall, $Bo=\rho g R_{crucible}^2/\sigma$ is the Bond number, σ, ρ, and g are the surface tension coefficient, the density and the gravity acceleration respectively. An additional parameter z_0 plays a role of Lagrange multiplier and is used to satisfy the restriction (2).

According to the vendor provided data, the surface tension coefficient of all four oils is approximately 0.02 N/m, and their density varies between 860 and 960 kg/m^3 [9]. Therefore, the values of the Bond number change mainly due to the characteristic length, and are estimated as ≈ 170 and ≈ 666 for the smaller and larger setups, respectively. We conducted several experiments to estimate wetting angle of silicone oils on a sapphire surface and found that the angle varies between 8° and 12°.

The problem (1)–(4) is discretized using central finite differences, after which the set of unknowns consists of N values of z at the grid points $r_i, i=1,2,\ldots N$, and the unknown value of z_0. The resulting system of non-linear algebraic equations is solved by the Newton method that converges within 40 iterations.

Examples of the calculated meniscus shapes are shown in Fig. 2a,b for the case of smaller crucible and radius of the crystal dummy 10 mm. The Bond number value was 170. The wetting angle on the crucible wall was varied to see its influence on the

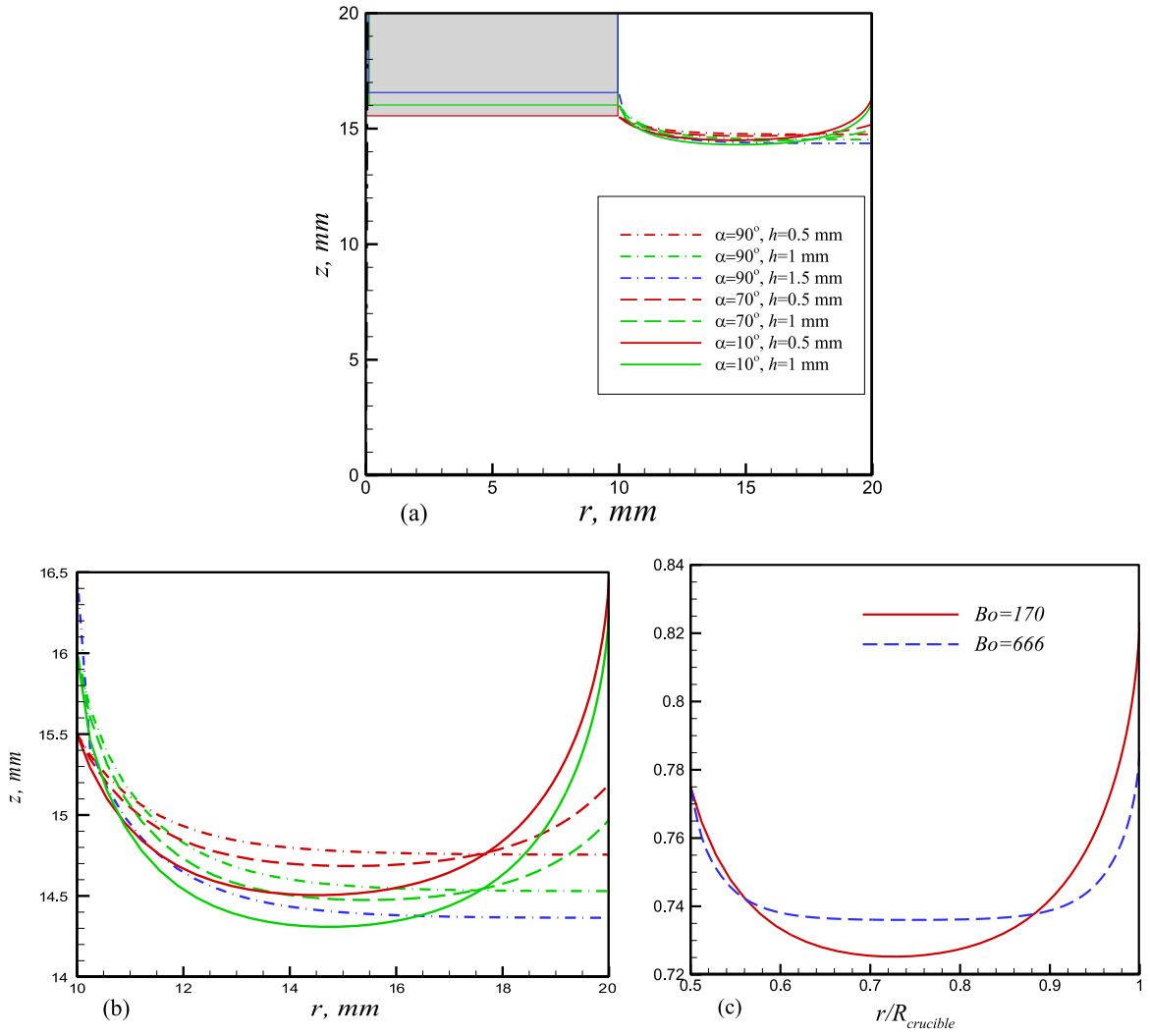

Fig. 2. (a) Shapes of the capillary menisci calculated for a smaller crucible at different heights and wetting angles at the crucible wall, $A=0.75$, $Bo=170$. The horizontal color lines show position of the crystal dummy bottom corresponding to the shape of the same color. (b) Shapes of the frame (a) zoomed in the z–direction. (c) Comparison of the menisci scaled by $R_{crucible}$ and calculated at $Bo=170$ and 680. (For interpretation of the references to color in this figure legend, the reader is referred to the web version of this article.)

meniscus shape. Fig. 2a shows the menisci in the proportional scaling in radial and axial coordinates. The colored horizontal lines indicate position of the dummy lower surface at three different meniscus heights. In Fig. 2b the axial coordinate is zoomed in to distinguish better between different cases. This allows us to see the meniscus shape changes when the wetting angle is decreased from 90° to 10°.

At the height of the meniscus of 1.5 mm ($h = 0.075$) we could obtain a smooth solution only for wetting angle at the crucible wall equal to 90°. This means that the meniscus already attains shapes sketched by the curves 3 and 4 in Fig. 1, which cannot be computed using above procedure.

The effect of the Bond number is illustrated in Fig. 2c. The two curves there are calculated for parameters of the smaller and the larger setups and then are scaled by $R_{crucible}$. The relative meniscus height, radii ratio and the aspect ratio in both cases are 0.025, 0.5 and 0.75, respectively. The wetting angle was 10°. We observe that at larger Bond number the central part of the meniscus tends to a horizontal surface, while its end parts change steeper. Such a difference in the upper surface shape can affect the flow pattern, as well as its stability properties.

4. Results

4.1. Main experimental results

In addition to the dimensionless parameters introduced above, the flow is governed by the Prandtl number $Pr = \nu/\chi$, the Grashof number $Gr = g\beta\Delta T R^3_{crucible}/\nu^2$, and the Marangoni number $Ma = MnPr$, where $Mn = -\gamma\Delta T R_{crucible}/\rho\nu^2$. Here χ is the thermal diffusivity, g is the gravity acceleration, β is the thermal expansion coefficient, and $\gamma = d\sigma/dT$ – the parameter describing the dependence of the surface tension coefficient σ on the temperature. As it was done in our previous studies [6–8], the crucible radius is chosen as the length scale. It is a convenient choice because the crucible radius is the only length that remains constant for all the experiments in a certain setup. The thermophysical parameters of silicone oils, as provided by vendor, can be found in [9]. As was already argued in [6], for our experimental setups $Mn \ll Gr$, the ratio Mn/Gr is of the order 10^{-2}–10^{-3}, so that the thermocapillary effect is assumed to be negligibly small. At the same time, the effect of the meniscus height is expected to be noticeable, as it was already reported in [4,5]. Also, judging by the menisci shape at different Bond numbers, the effect of the latter should be examined. In particular, different Bond numbers can be a reason of

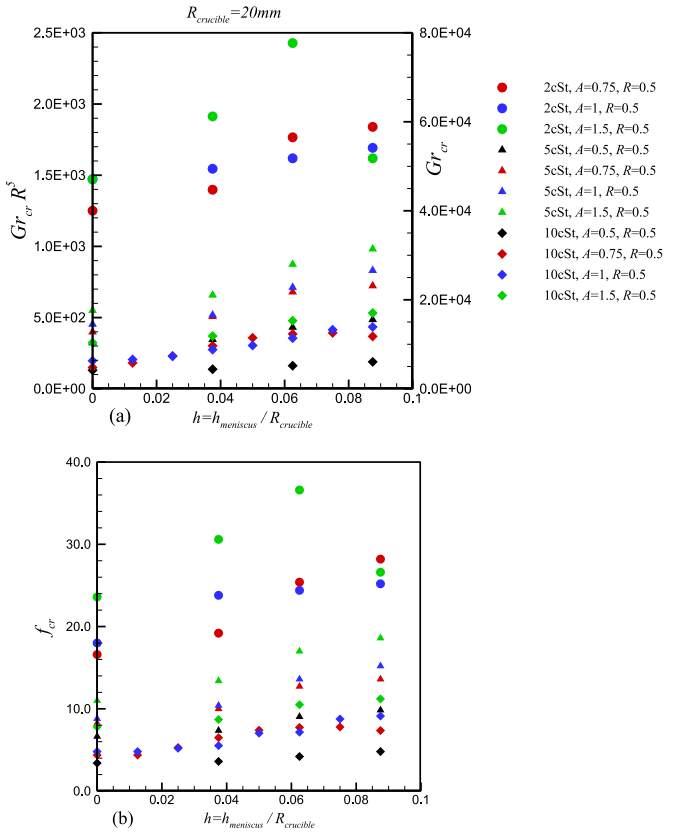

Fig. 3. Results for the smaller setup: measured critical points via dimensionless parameters: the Grashof number (a) and the dimensionless critical frequency (b) versus the relative meniscus heights for different silicone oils and aspect ratios. R=0.5. The results for silicone oils with 2, 5, and 10 cSt viscosity are shown by circles, triangles (Δ) and diamonds, respectively. The results for the melt aspect ratios 0.5, 0.75, 1, and 1.5 are colored by black, red, blue, and green, respectively. Radii ratio is R=0.5. (For interpretation of the references to color in this figure legend, the reader is referred to the web version of this article.)

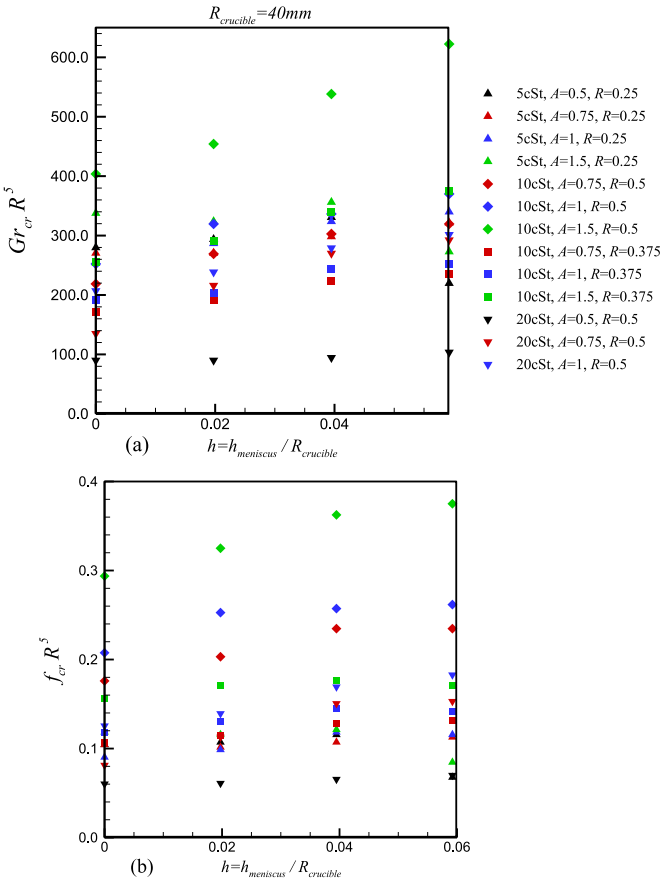

Fig. 4. Results for the larger setup: measured critical points via dimensionless parameters: the Grashof number (a) and the dimensionless critical frequency (b) versus the relative meniscus heights for different silicone oils, aspect and radii ratios. The results for silicone oils with 5, 10, and 20 cSt viscosity are shown by triangles (Δ), diamonds and squares, and triangles (∇), respectively. The results for the melt aspect ratios 0.5, 0.75, 1, and 1.5 are colored by black, red, blue, and green, respectively. The diamonds and squares show results for, respectively, R=0.5 and 0.375. (For interpretation of the references to color in this figure legend, the reader is referred to the web version of this article.)

the absence of exact scaling of critical parameters measured in the two setups.

The results of all the measurements are collected in Figs. 3 and 4 for the smaller and larger setup, respectively. To distinguish between different silicone oils and different aspect ratios, the symbols on these and other graphs are organized as follows. The results for silicone oils with 2, 5, 10, and 20 cSt viscosity are shown by circles, delta-triangles (Δ), diamonds/squares, and gradient-triangles (∇), respectively. The results for the aspect ratios A = 0.5, 0.75, 1, and 1.5 are colored as black, red, blue and green, respectively. When the results obtained on both setups are shown in the same graph (Figs. 5 and 6), the symbols corresponding to the small setup are hollow, while those corresponding to the large setup are filled. To collect all the experimental points on the same graph, in Fig. 4 the Grashof number and the oscillations frequency are additionally multiplied by R^5. In Fig. 3 we also show the left vertical axis for GrR^5 to allow for comparison between the two setups, as well as the right axis for Gr, to illustrate range of the critical values. We observe that with the increase of the meniscus height h from the zero level, the critical Grashof number (the critical temperature difference ΔT_{cr}), as well as the oscillation frequencies increase. For a very viscous working liquid (20 cSt, Pr=206), the increase is within 20%, however, for less viscous one (e.g., 2 cSt, Pr=23.9), and more relevant for molten optical materials, the difference can reach 100%. This happens, for example, in the smaller crucible setup with A = 1 (Fig. 5a). The reason of this increase will be discussed below.

4.2. Similitude of the two experimental setups

The initial idea of measurements in two independent setups, whose geometrical parameters scale exactly as 1:1.9, was verification of the results via the similitude theory. Thus, assuming that the effects of the thermocapillarity and the menisci shape are negligibly small, and all the other parameters except the Grashof number are exactly equal and do not depend on the temperature, one would expect that the instability in both setups will set in at the same Grashof number. Since the Grashof number is proportional to $R^3_{crucible}$, and viscous and heat diffusive time scales are $\nu/R^2_{crucible}$ and $\chi/R^2_{crucible}$, respectively, this means that for the two setups the critical temperature differences between the crucible and the crystal dummy is expected to relate as $1{:}1.9^3$, and the corresponding oscillation frequencies as $1{:}1.9^2$. In fact, only part of our results can be compared in this way. In the smaller setup we cannot conduct measurements with very viscous oils because the critical temperature difference exceeds 50 °C, so that the oil starts to evaporate. In larger setup we have an opposite problem with less viscous oils: the critical temperature difference becomes smaller than 1 °C, which makes it impossible to carry out accurate measurements (see [11] for the details). Also, in the larger setup we were able to increase the relative meniscus height only to h = 0.06, while in the smaller one the menisci remained stable up to almost h = 0.1. This is why the only comparison available

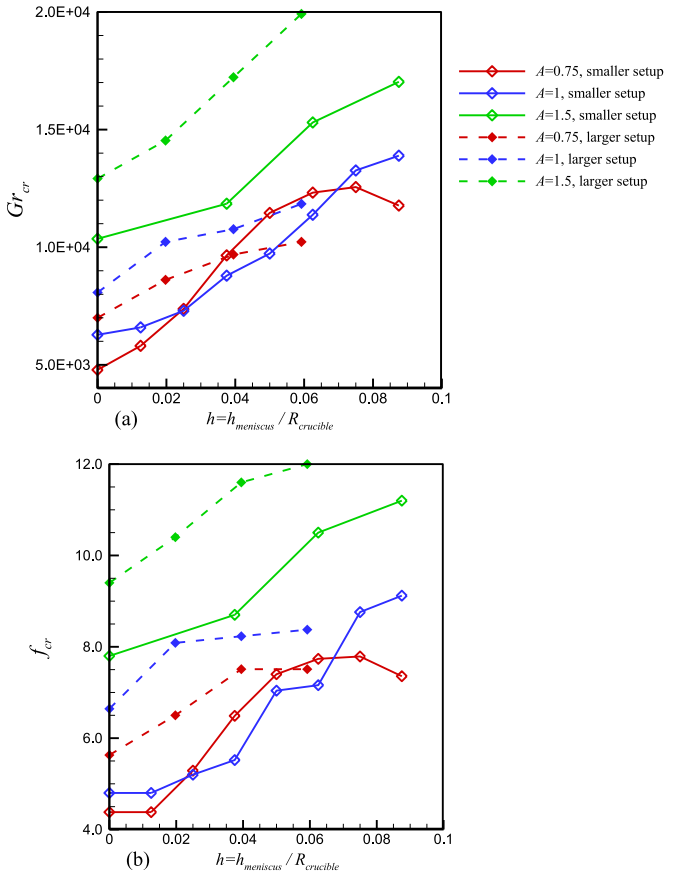

Fig. 5. Comparison of critical parameters measured for $Pr = 99.3$, $R = 0.5$ in smaller (solid lines) and larger (dash lines) setups: the Grashof number (a) and the dimensionless critical frequency (b) versus the relative meniscus heights for different aspect ratios. The shapes and the colors of symbols correspond to Figs. 3 and 4. Symbols denoting the smaller setup are hollow. (For interpretation of the references to color in this figure legend, the reader is referred to the web version of this article.)

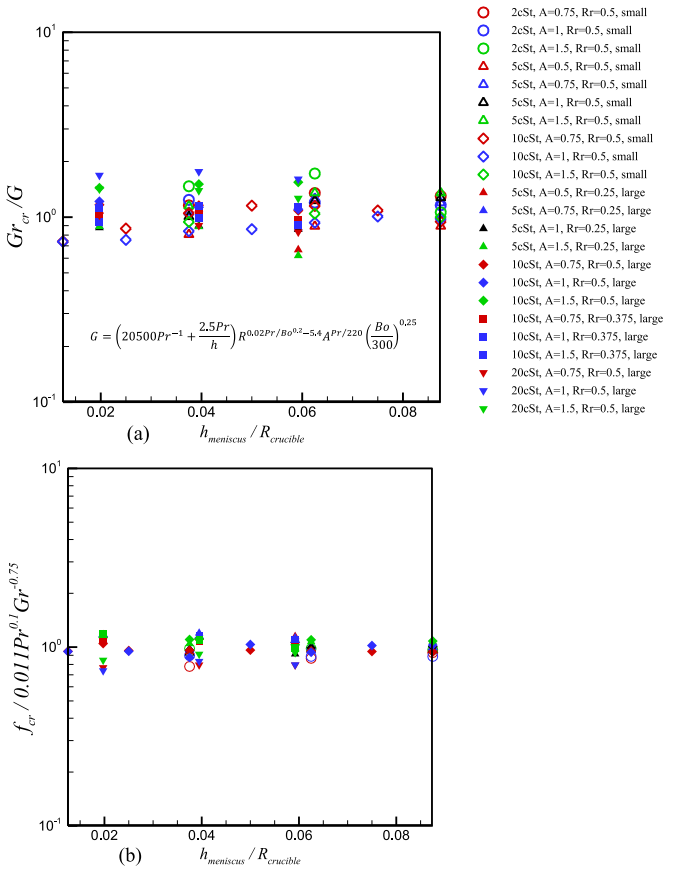

Fig. 6. Scaled critical Grashof number (a) and dimensionless critical frequency (b) versus the relative meniscus height with varied aspect and radii ratios, Bond and Prandtl numbers. The symbols and the colors are same as in Figs. 3 and 4. The results for small crucible are shown by hollow symbols. (For interpretation of the references to color in this figure legend, the reader is referred to the web version of this article.)

corresponds to the fixed values of $Pr = 99.3$ and $R = 0.5$. For these two fixed values we expected to observe same or close dependencies $Gr_{cr}(h, A)$ in both setups. The comparison is shown in Fig. 5. Curves and symbols of the same color correspond to the same aspect ratio and should be compared.

We start to discuss the comparison from the zero meniscus height ($h = 0$), at which the meniscus is attached to the crystal dummy side, as is sketched by the curve 1 of Fig. 1. The cylindrical surface of the crystal dummy affects the meniscus as a plane wall if the liquid capillary length $\sqrt{\sigma/\rho g}$ is much smaller than the cylinder radius [12]. In our case the capillary length can be estimated as 1.5 mm for all the oils, so that the inequality $\sqrt{\sigma/\rho g} \ll R_{crystal}$ is not too accurate, especially for the smaller setup, where the crystal radius corresponding to Fig. 5 is 10 mm. This means that the results we intend to compare are altered not only by the Bond number, but also by the different meniscus shapes at the crystal/meniscus contact line. The critical Grashof numbers and the dimensionless critical frequencies measured on the larger setup are 20–40% larger than those measured on the smaller setup, which may be a result of the meniscus effect. Another possible reason of the difference is the temperature dependence of the thermophysical parameters, whose effect is noticeably stronger in the smaller setup where approximately 7 times larger temperature differences are needed to arrive to the instability threshold. Effect of the temperature dependence can be an objective of a thorough computational modeling, but is out of the scope of this study.

Apparently, difference of the menisci shape is not a single reason that can cause the difference of critical parameters. The ratio Mn/Gr decreases as $R_{crucible}^{-2}$, so that it is 3.61 times smaller for the larger setup. The main circulation of the melt flow is due to the buoyancy forces. The flow rises near the hot crucible wall and descends below the cold crystal. At the capillary surface the flow direction is from the crucible wall to the crystal dummy. The thermocapillary force drives the flow from the hot crucible to the cold crystal, thus intensifying the main buoyant circulation. If this intensification is stronger in the smaller setup, it is expected to have a destabilizing effect, so that the critical temperature difference together with the critical Grashof number will decrease. As a result, the critical Grashof numbers measured on the smaller setup will be smaller. The latter is observed in Fig. 5 for the zero meniscus height. As mentioned above, another reason can be related to the temperature dependence of all the thermophysical properties.

With the increase of the meniscus height from zero the critical Grashof number and the dimensionless oscillation frequency grow in both experimental facilities, while the values measured using the smaller setup remain smaller. The average slopes of the increase of the Gr_{cr} and f_{cr} at $A=1$ and 1.5 are apparently close to each other for both facilities, small and large, in the same range of dimensionless variations of the meniscus height, $0 < h < 0.06$. At $A=0.75$ the behavior of the slope is essentially non-monotonic and it is difficult to define the average slope. This indicates on a certain qualitative similarity, however the results for two setups remain different and continue to exhibit the absence of definite similitude. Apparently, all the reasons for that, discussed above, can be

repeated for the non-zero meniscus height.

In the smaller setup, for the smallest melt aspect ratio $A = 0.75$ and $h > 0.06$, we observe decrease in both values. A similar decrease is observed for the 2 cSt oil at $A = 1.5$ (green circles in Fig. 3). Since the meniscus shape is independent of the melt depth, this decrease can be a combined effect of all the phenomena involved, and probably can be related to a change of the meniscus from the shape 2 to the shapes 3 or 4 sketched in Fig. 1. Unfortunately, we were unable to make precise measurements of the meniscus shape.

4.3. Scaling of the critical parameters

Using the above experimental data we made an attempt to extend the scaling functions reported recently in [6], and to add there new dimensionless values of the meniscus height and the Bond number. We have found, however, that out present data for the critical Grashof number (critical temperature difference) scatters stronger than that of [6], probably because of slight differences of the surface tension and the wetting angles corresponding to different oils. It is emphasized that the scaling below is found only for those parameters at which we can assume the meniscus of shape 2. Therefore, we take into account only experimental points of Figs. 3 and 4, for which $h > 0$, and increase of the Grashof number with the meniscus height is observed. The best fit we could find is described by the following relation (Fig. 6a)

$$Gr_{cr} \approx \left(20500Pr^{-1}+\frac{2.5Pr}{h}\right)R^{0.02Pr/Bo^{0.2}-5.8}A^{Pr/110}\left(\frac{Bo}{300}\right)^{0.25} \quad (5)$$

At the same time, scaling of the oscillations frequency is not explicitly dependent on the capillarity parameters and as in [6] is described by (Fig. 6b)

$$f_{cr} \approx 0.011Pr^{-0.1}Gr_{cr}^{0.75} \quad (6)$$

Note that in spite of only two governing parameters involved in the above equation, the critical Grashof number depends on all other parameters via Eq. (5), so that the critical frequency is also a function of all the governing parameters. Clearly, all the conclusions and discussion of [6] related to the scaling relations remain correct also for the present results. In particular, the critical Marangoni number Ma_{cr}, that describes the thermocapillary effect, is scaled by [6]

$$Mn_{cr} = \frac{Gr_{cr}}{Bo}\frac{(-\gamma)}{\beta\sigma},\ Ma_{cr} = Mn_{cr}Pr \quad (7)$$

4.4. Discussion and additional model experiments

Basing on our previous results [6–9], for the following discussion we assume that in the most cases the instability sets in due to formation of cold plumes at the crystal dummy cold surface. As explained in [13], the instability sets in due to accumulation of cold liquid below the cold crystal dummy until an unstable vertical temperature gradient reaches its critical value, after which the Rayleigh-Bénard instability mechanism sets in. In view of this explanation, growth of the critical Grashof number with the increasing meniscus height can be explained as follows. Inside the meniscus the flow is very weak, which leads to a weaker convective mixing of the cold liquid attached to the dummy and bounded by the meniscus with the hot liquid advected from the crucible wall. The mixing is weakened further when the meniscus height is increased. A weaker mixing results in a smoother temperature profile, so that change of the temperature along the vertical axis becomes less steep. Therefore, higher temperature difference is necessary to generate appropriate conditions for development of instability in the melt. As a result, the instability threshold takes place at larger difference ΔT_{cr} of the hot and cold boundaries temperature. We can speculate further that when the meniscus attains the shapes 3 or 4 (Fig. 1), the liquid volume inside the meniscus decreases. Since a smaller liquid volume should be mixed, the mixing inside the meniscus can be intensified leading to a decrease of the critical temperature difference. This might explain the saturation of the dependence of the critical Grashof number on dimensionless meniscus height that occurs at higher values of h.

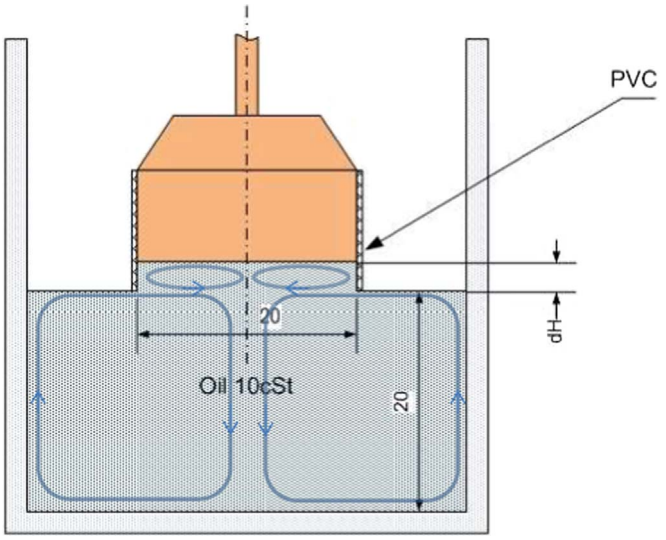

Fig. 7. Sketch of the model experiment with a PVC tube attached to the crystal dummy. All the sizes are given in millimeters.

To verify the above explanation, we performed another model experiment, in which a PVC tube was attached to the crystal dummy, as is shown in Fig. 7. This experiment was carried out in a smaller facility with 10 cSt oil, keeping the radii and aspect ratios at $R = 0.5$ and $A = 1$. In this experiment a column of oil inside the PVC tube replaces the meniscus. When the height of the column was 1.75 mm, the temperature oscillations appeared at the temperature difference of 11 °C, while with the meniscus of the same height the critical temperature difference was 17.7 °C. This quite surprising reduction of ΔT_{cr} can be caused by a better mixing inside the PVC tube. Really, inside a tube with no-slip boundaries one can expect appearance of reversed circulations, as is shown schematically in Fig. 7. Flow inside these circulations is faster than that inside the meniscus, which yields better mixing and reduction of the critical temperature difference.

In the next experiment we sharply increased the height of the oil column inside the tube to 4 mm, which resulted in a steep increase of the critical temperature difference to 33.5 °C. Clearly, the inverse circulations in a taller column inside the PVC tube become slower, which slows down the mixing. As a result the oil column inside a tube produces an effect of a solid body with heat conductivity sharply reduced compared to that of the copper. This flattens the temperature gradient along the vertical axis, which leads to a sharp increase of ΔT_{cr}.

5. Conclusions

This experimental study was focused on the capillary meniscus effect on the instability of the model large-Prandtl-number Czochralski melt flows. The measurements were carried out by two independent and fully non-intrusive experimental techniques on

two experimental facilities whose sizes scaled as 1:1.9. The results are presented as dependencies of the critical Grashof number and the melt oscillations frequency on the meniscus height scaled by the crucible radius.

The results show that the critical Grashof number (the critical temperature difference) tends to increase with the increase of the meniscus height. The difference between results obtained for "short" and "tall" menisci is noticeable and sometimes can reach 100%. We argued that the flow stabilization at taller menisci takes place owing to a less intensive mixing of the cold liquid located below the cold dummy and the hot liquid advected from the crucible wall towards the cylindrical axis. This argument was supported by an additional qualitative experiment.

Finally, we extended the empirical relations for the critical Grashof number and oscillation frequency, reported in [6], to variable relative meniscus heights and Bond numbers.

Acknowledgment

The authors wish to acknowledge a kind contribution of experimental setup that Professor Dietrich Schwabe donated to our laboratory. This study was supported by the Israel Science Foundation (Grants 426/12 and 408/15) and in part by the Wolfson Family Charitable Trustpr/ylr/18921&18837.

References

[1] Th Duffar (Ed.), Crystal Growth Processes Based on Capillarity, Wiley & Sons Ltd., Chichester, UK, 2010.
[2] D. Schwabe, E. Uecker, M. Nernhagen, Z. Galazka, J. Cryst. Growth 335 (2011) 138.
[3] A.D.W. Jones, J. Cryst. Growth 63 (1983) 70.
[4] P. Hintz, D. Schwabe, H. Wilke, J. Cryst. Growth 222 (2001) 343.
[5] P. Hintz, D. Schwabe, J. Cryst. Growth 222 (2001) 356.
[6] E. Miroshnichenko, E. Kit, A. Yu Gelfgat, J. Cryst. Growth 438 (2016) 38.
[7] V. Haslavsky, E. Miroshnichenko, E. Kit, A. Yu Gelfgat, J. Cryst. Growth 318 (2011) 156.
[8] V. Haslavsky, E. Kit E, A. Yu Gelfgat, Acta Phys. Pol., Pt. A 124 (2013) 193.
[9] M. Teitel, D. Schwabe, A. Gelfgat, J. Cryst. Growth 310 (2008) 1343.
[10] H.J. Scheel, P. Capper (Eds.), Crystal Growth Technology, Wiley VCH, Darmstadt, 2008.
[11] V. Haslavsky, E. Kit E, E. Miroshnichenko, A. Yu Gelfgat, Fluid Dyn. Mater. Process. 9 (2013) 209.
[12] C. Clanet, D. Quéré, J. Fluid Mech. 460 (2002) 131.
[13] A. Yu Gelfgat, J. Fluid Mech. 385 (2011) 377.